Electronic Supplementary Information

Anisotropic strain release in a thermosalient crystal: Correlation between the microscopic orientation of molecular rearrangements and the macroscopic mechanical motion

Tomohiro Seki,[a]* Takaki Mashimo,[a] Hajime Ito[a,b]*

[a]Division of Applied Chemistry & Frontier Chemistry Center (FCC), Faculty of Engineering, Hokkaido University, Sapporo, Hokkaido 060-8628, Japan

[b]Institute for Chemical Reaction Design and Discovery (WPI-ICReDD), Hokkaido University, Sapporo, Hokkaido 060-8628, Japan.

seki@eng.hokudai.ac.jp
hajito@eng.hokudai.ac.jp

Contents |

1. General

All commercially available reagents and solvents are of reagent grade and were used without further purification unless otherwise noted. Solvents for the synthesis were purchased from commercial suppliers, degassed by three freeze-pump-thaw cycles and further dried over molecular sieves (4 Å). NMR spectra were recorded on a JEOL JNM-ECX400P or JNM-ECS400 spectrometer (^{1}H: 400 MHz; ^{13}C: 99.5 MHz) using tetramethylsilane and $CDCl_3$ as internal standards, respectively. Emission spectra were measured by using an Olympus fluorescence microscope BX51 equipped with Hamamatsu photonics multichannel analyzer PM-12. DSC measurements were recorded on a SII DSC 7020 heat flux meter or TA Instruments DSC2500. The powder samples were loaded into an aluminum pan and sealed and were cooled inside the apparatus. Elemental analyses and low- and high-resolution mass spectra were recorded at the Global Facility Center at Hokkaido University. Photographs were obtained using Olympus BX51 or SZX7 microscopes with Olympus DP72, Nikon D5100 or RICOH CX1 digital cameras. Powder diffraction data were recorded at on a Rigaku SmartLab diffractometer with Cu-K_α radiation and D/teX Ultra detector covering 5–60° (2θ). TCU 110 Temperature Control Unit (Anton-Paar) was used for the cooling the sample on the sample stage. A cooling/heating stage on JHC 10002L was used for temperature changes of solid samples. High-speed camera recording was performed using a Photron FASTCAM Mini AX.

X-ray diffraction analyses: Single crystal X-ray structural analyses were carried out on a Rigaku XtaLAB PRO MM007 diffractometer using graphite monochromated Mo-K_α radiation. The structure was solved by direct methods and expanded using Fourier techniques. Non-hydrogen atoms were refined anisotropically. Hydrogen atoms were refined using the riding model. All calculations were performed using the CrystalStructure crystallographic software package except for refinement, which was performed using SHELXL-2014.[1] Simulated powder patterns were generated with Mercury 3.10[2] from the structures determined by the single-crystal diffraction analyses.

2. Synthesis

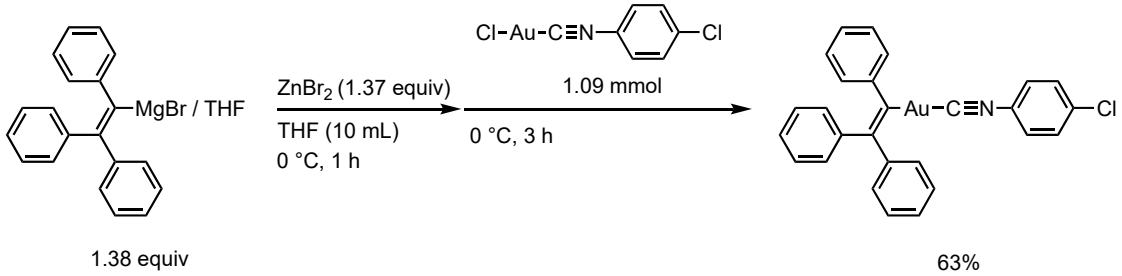

1.38 equiv

63%

A powder of zinc bromide (335.9 mg, 1.49 mmol) was placed in an oven-dried two-neck flask. The flask was connected to a vacuum/nitrogen manifold through a rubber tube. It was evacuated and then backfilled with nitrogen. This cycle was repeated was three times. THF (10 mL) was then added in the flask through the rubber septum using a syringe and stirred at 0 ℃. A triphenylethenemagnesium bromide reagent in THF (6.8 mL, 0.22 M, 1.50 mmol) was then added to the reaction mixture using a syringe and stirred at 0 ℃ for 1h. Then, a powder of chloro(4-chlorophenyl isocyanide)gold(I) complex (403.8 mg, 1.09 mmol) was added and the mixture was stirred at 0 ℃ for 3h. After the reaction completion was monitored by TLC analysis, the reaction mixture was quenched by the addition of a phosphate buffer solution and then extracted with CH_2Cl_2 three times. The organic layers were collected and dried over $MgSO_4$. After filtration, the solvent was removed *in vacuo*. Further purification by column chromatography (SiO_2, EtOAc/hexane) gave an analytically pure yellow solid of **1** (406.8 mg, 0.69 mmol, 63 %). ^{1}H NMR (400 MHz, $CDCl_3$, Fig. S22, δ): 6.88–7.12 (m, 11H), 7.18–7.35 (m, 2H), 7.36–7.46 (m, 4H), 7.59–7.65 (m, 2H). ^{13}C NMR (100 MHz, $CDCl_3$, Fig. S23, δ): 123.7 (*C*H), 125.6 (*C*H), 126.3 (*C*H), 127.3 (*C*H), 127.5 (*C*H), 128.0 (*C*H), 129.3 (*C*H), 130.0 (*C*H), 130.4 (*C*H), 131.6 (*C*H), 137.5 (*C*), 144.3 (*C*), 149.1 (*C*), 149.6 (*C*), 150.7 (*C*), 161.2 (*C*), 168.9 (*C*). MS(*m*/*z*): $[M+Na]^+$ calcd for $C_{27}H_{19}AuClNNa$, 612.07692; found, 612.07692. Anal. Calcd for $C_{27}H_{19}AuClN$: C, 54.98; H, 3.25; N, 2.37; found: C, 54.97; H, 3.09; N, 2.31.

3. Photograph of the crystals of 1 and the emission properties of 1a and 1b

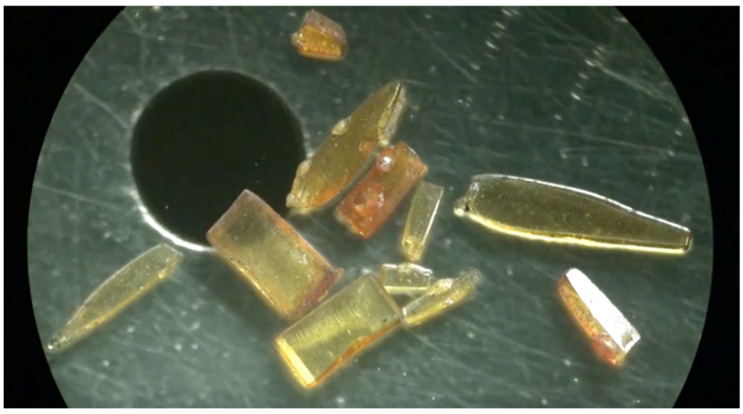

Fig. S1 Photograph of crystals **1a** under ambient condition.

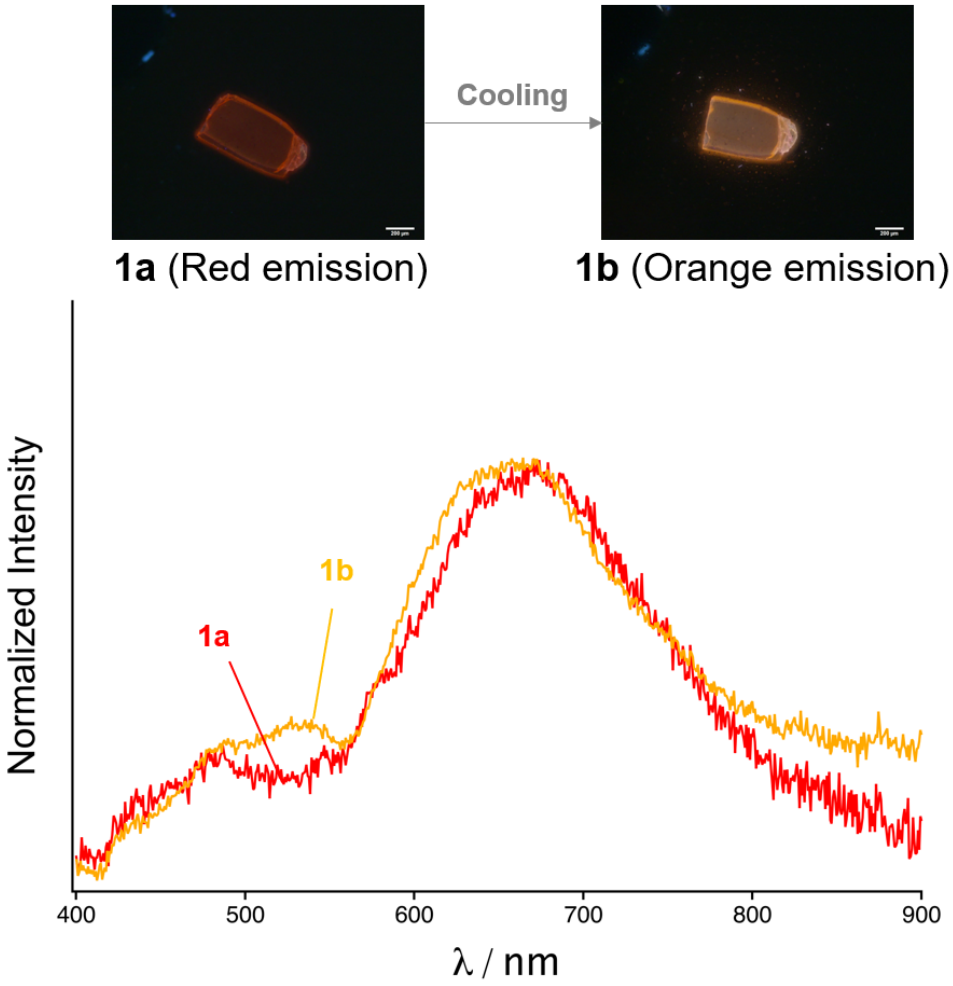

Fig. S2 Photographs of **1a** and **1b** taken under UV light (365 nm). Emission spectra of **1a** at 20 °C (red line) and **1b** at −150 °C (orange line) under excitation at 365 nm.

4. Observation of the thermosalient effect of 1

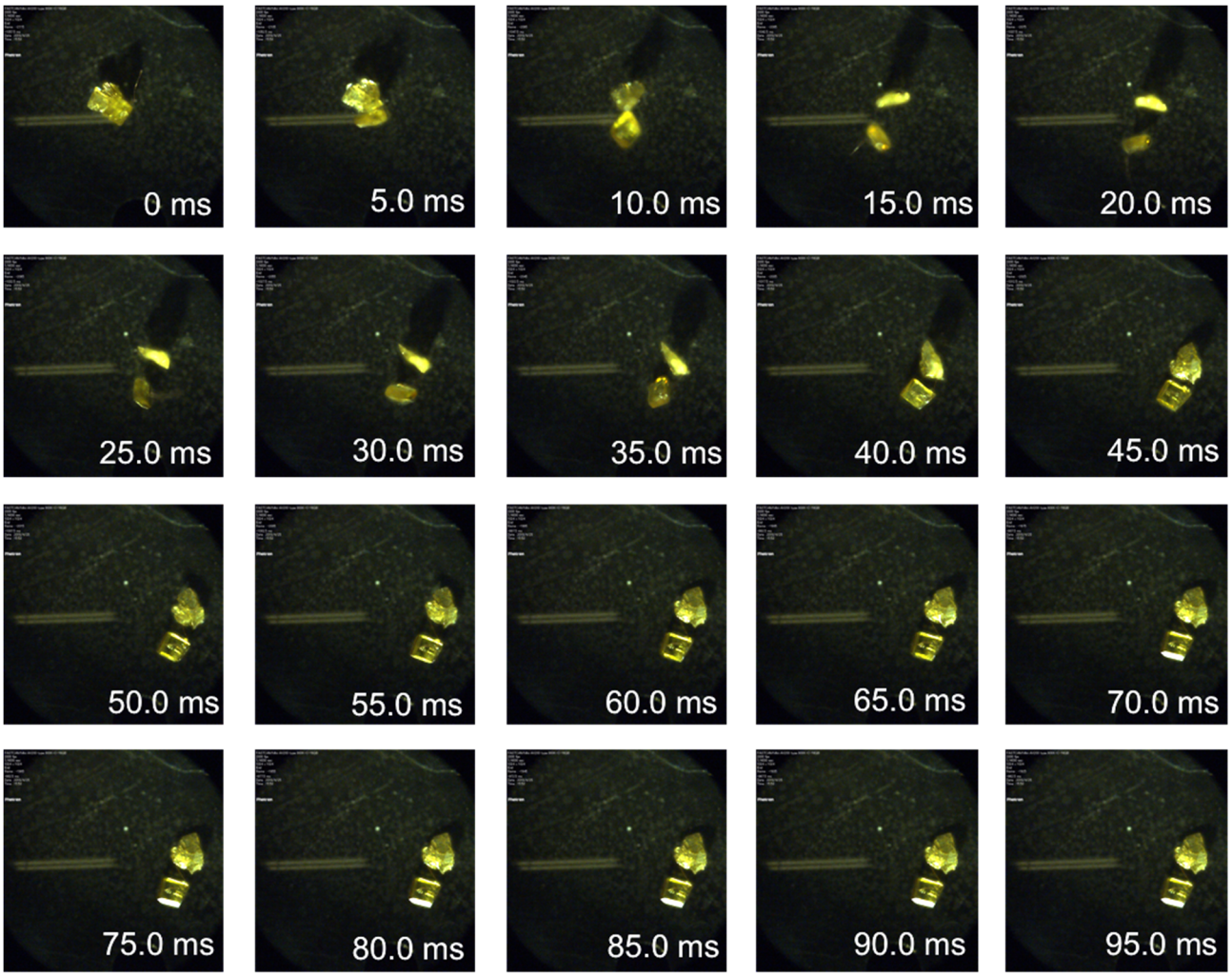

Fig. S3 Photographs of **1** upon cooling (30 °C/min), derived from a movie using a high-speed camera (2000 fps). The approximate temperature is −90 °C. See also the Supplementary Movies S1–S3.

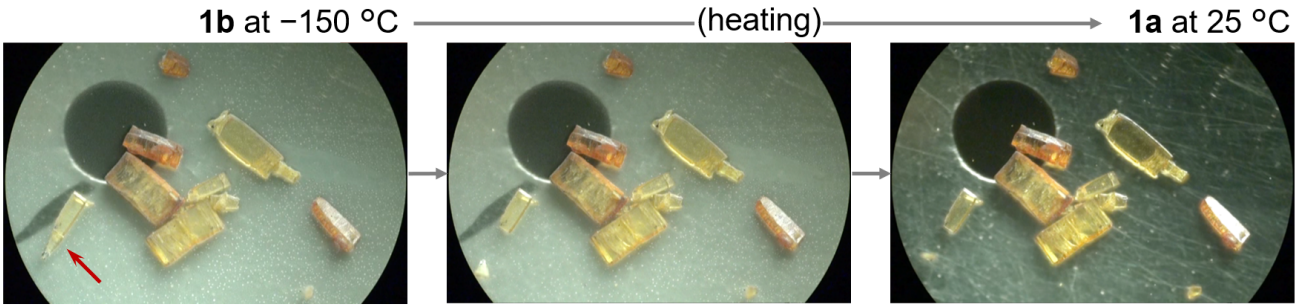

Fig. S4 Photographs showing thermosalient effect of **1** upon heating from −150 °C at 30 °C/min. Red arrow shows the crystal which jump during this observation.

5. Evaluation of the thermosalient properties of the powder samples of 1

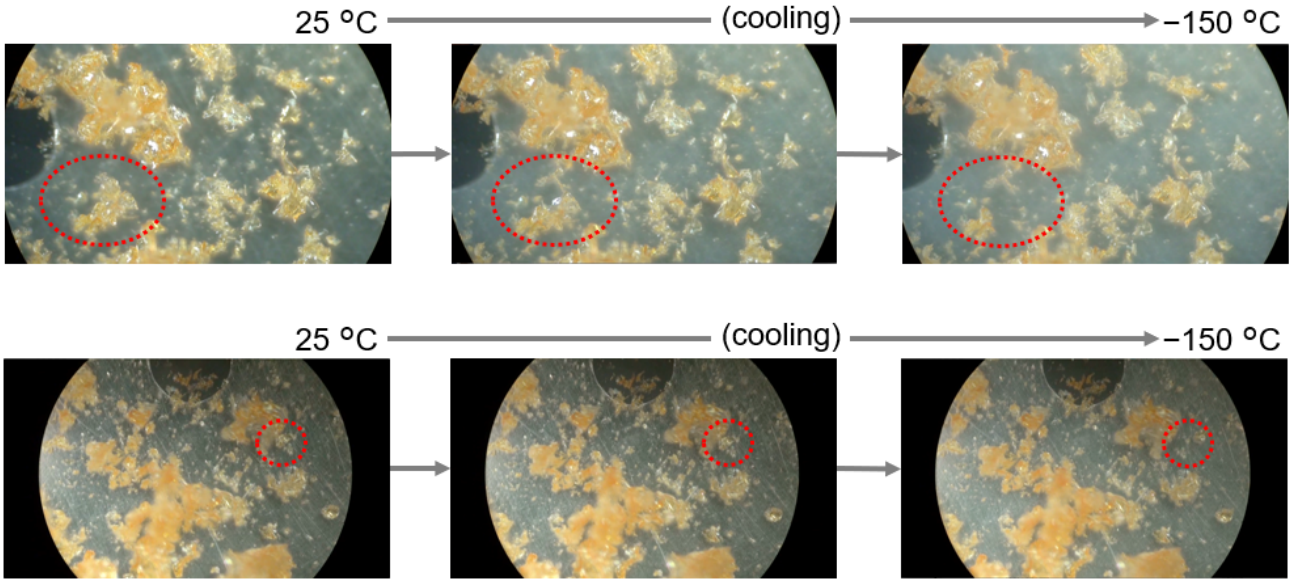

Fig. S5 Photographs showing the absence of the thermosalient effect of the powder forms of **1** upon cooling from 25 °C at 30 °C/min. Red dotted circles show slight dislocation of the samples but no clear jumping was observed.

6. Bending and splitting behaviors of 1 upon cooling

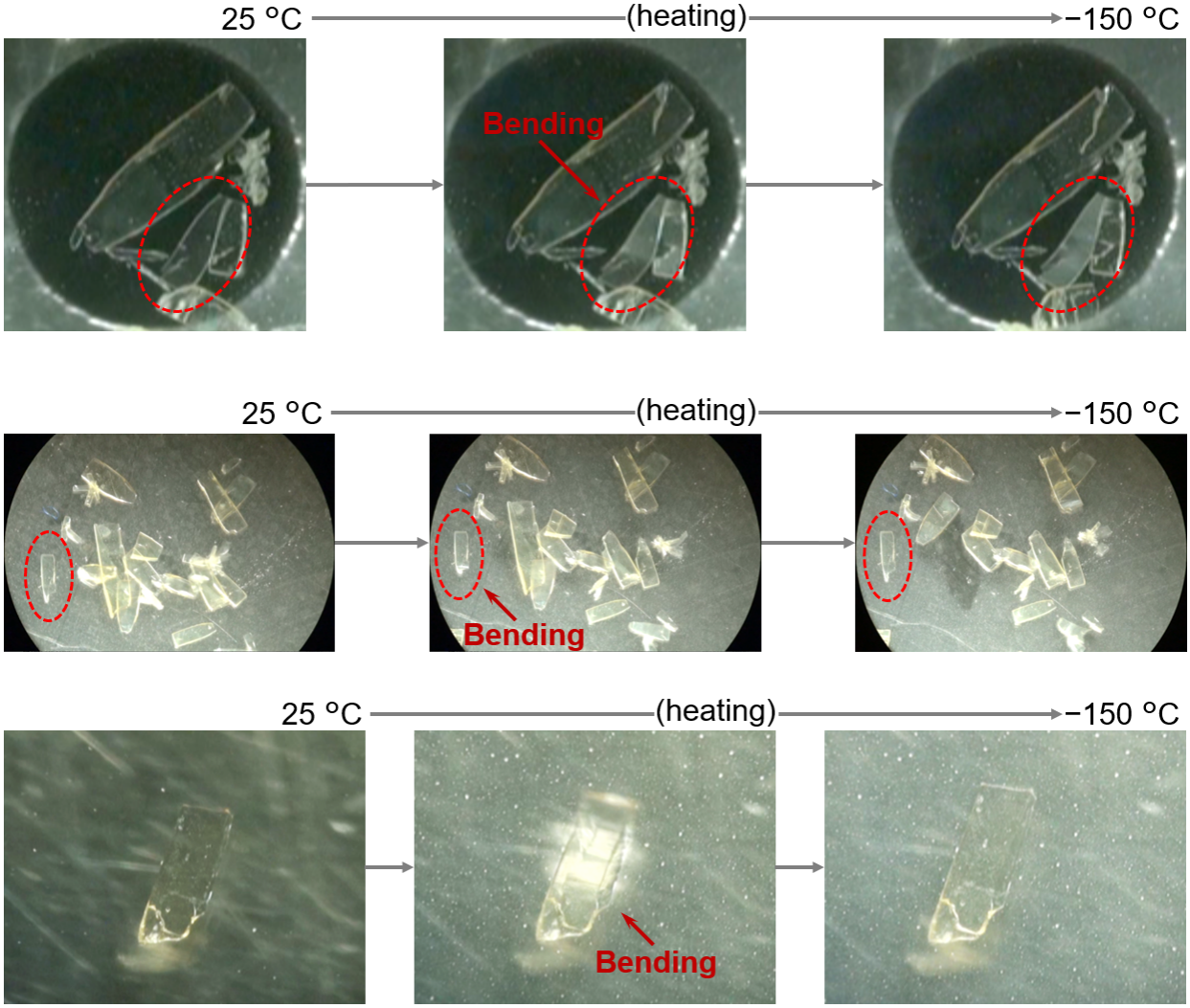

Fig. S6 Photographs showing the crystal "bending" along the major crystal axis of **1** (denoted by red arrows) upon cooling at 30–50 °C/min. See also the Supplementary Movies S4 and S5.

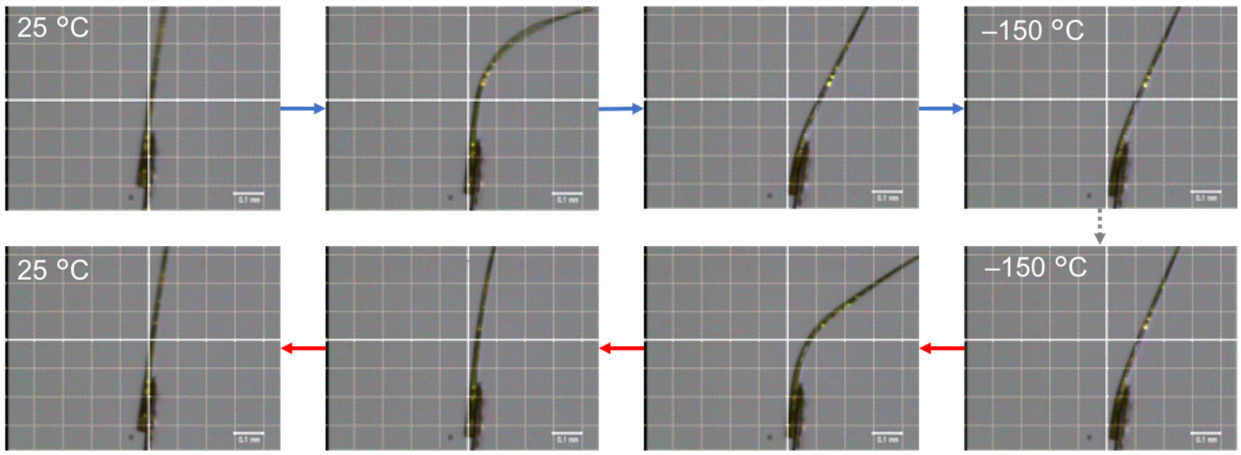

Fig. S7 Photographs of the crystal of **1** on a goniometer head showing bending along the major crystal axis upon cooling (~150 °C/min) and then heating (~150 °C/min) using a flow of nitrogen gas.

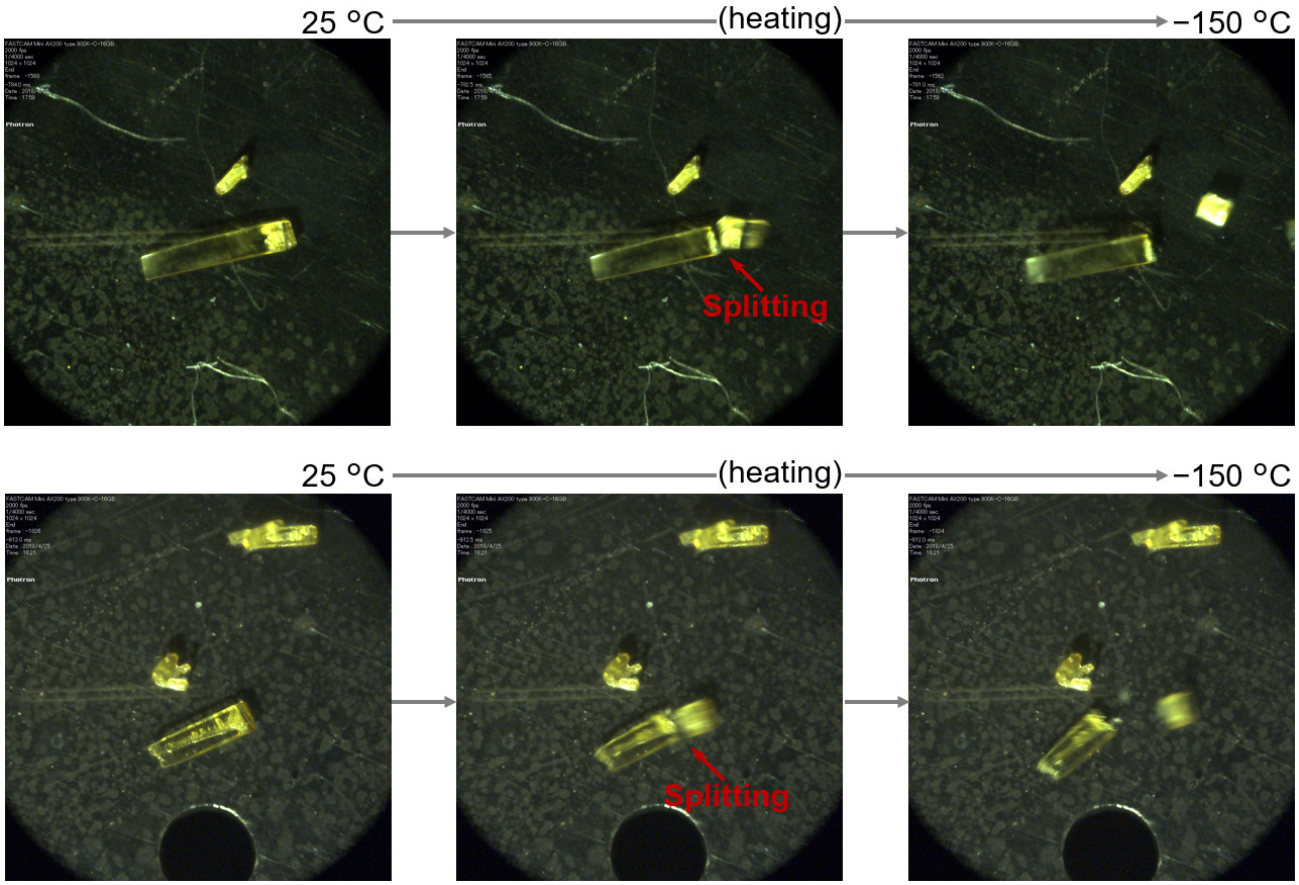

Fig. S8 Photographs showing the crystal "splitting" perpendicular to the major crystal axis of **1** (denoted by red arrows) upon cooling at 50 (top) and 30 °C/min (bottom). These photos are derived from the high-speed camera recording (2000 fps). See also the Supplementary Movies S1, S6, and S7.

7. Single crystal structure analyses of 1

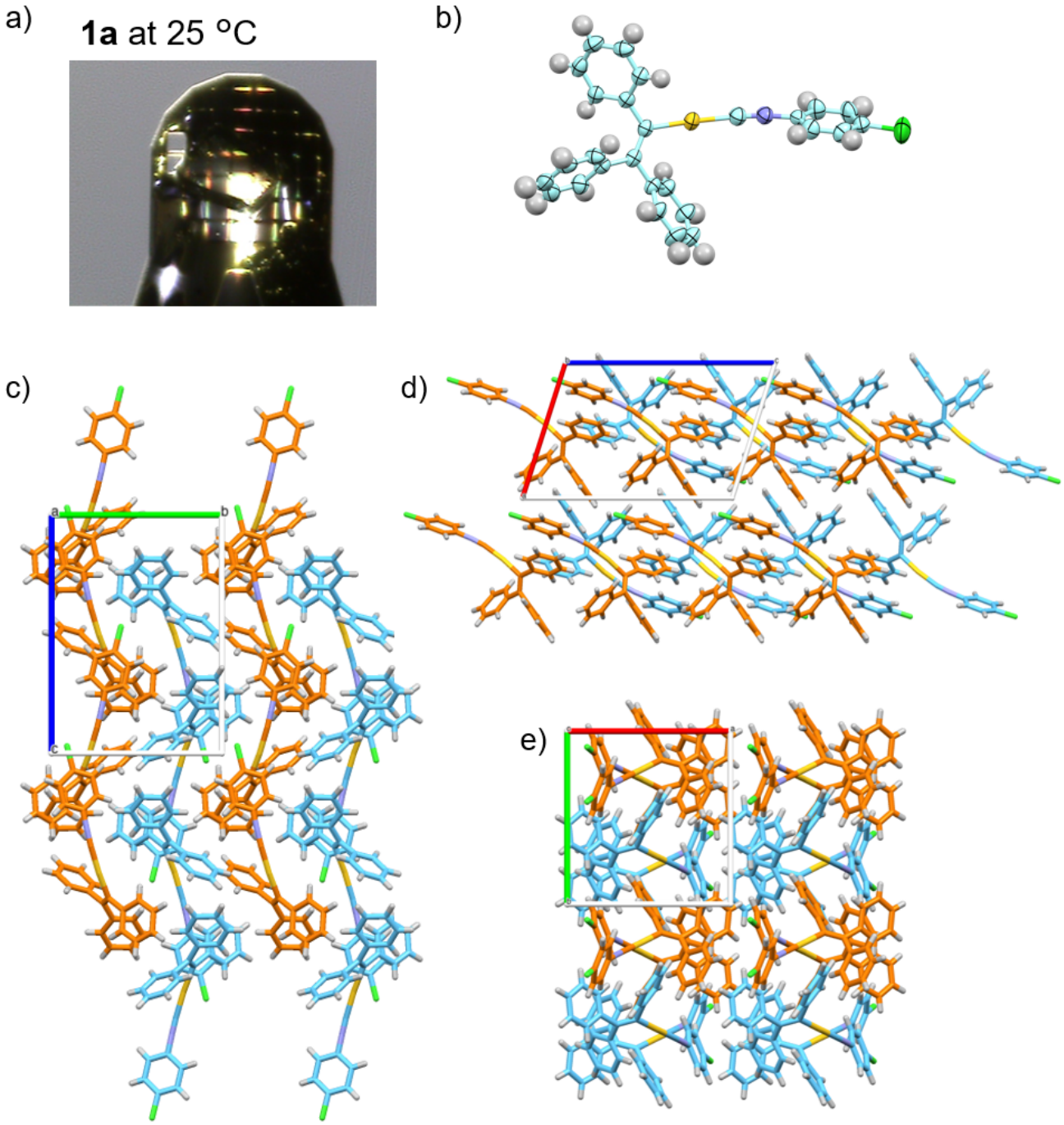

Fig. S9 a) Photograph of the single crystal of **1a** at 25 °C in which lots of Paraton oil was used to fix the crystals to decrease the probability of the crystals breaking upon subsequent cooling. Single crystal structure of **1a** at 25 °C which display b) a monomer and packing arrangements viewed along c) *a* axis, d) *b* axis, and e) *c* axis.

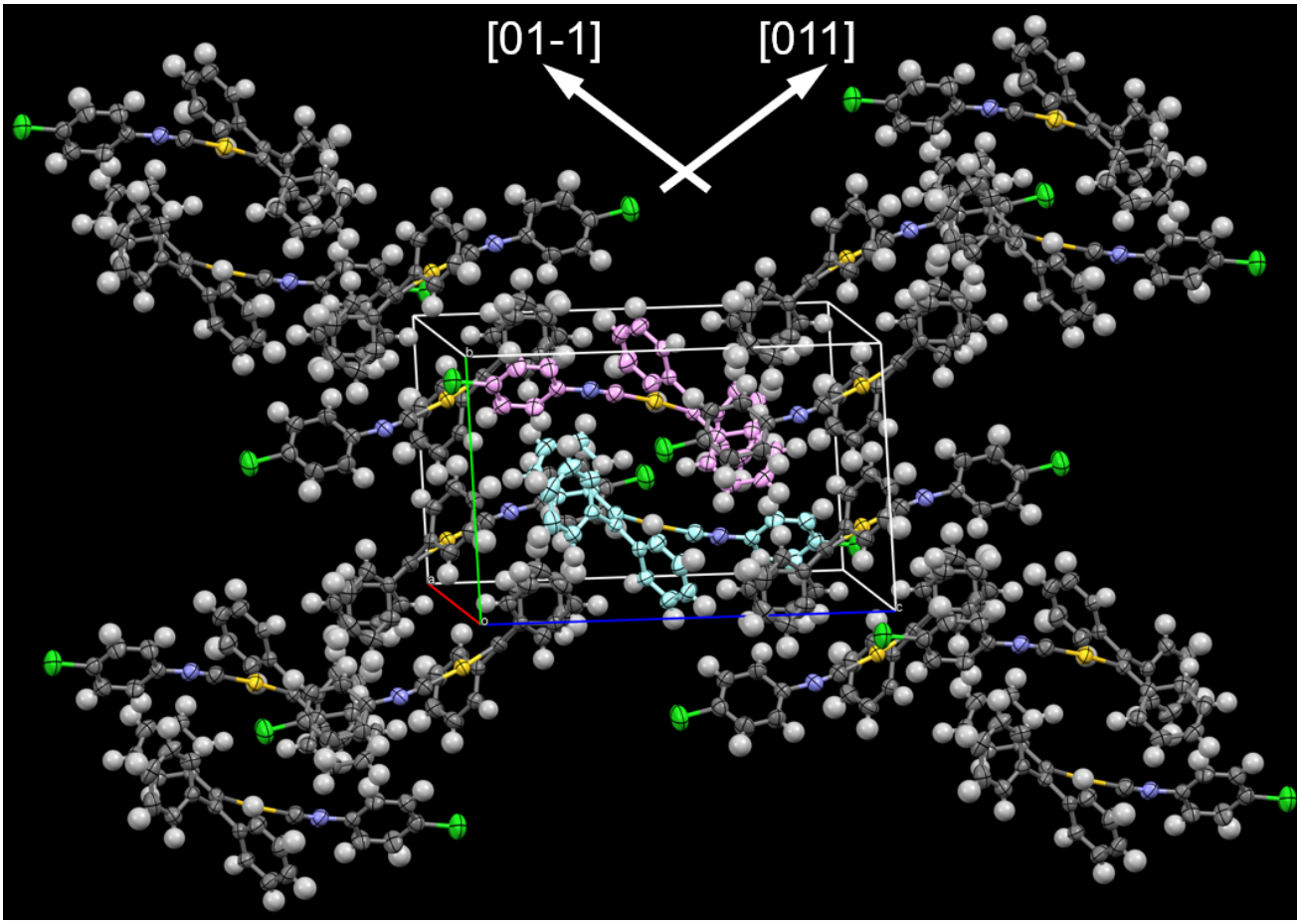

Fig. S10 Single crystal structure of **1a** at 25 °C. The molecular chains, formed through the extended π-π stacking interactions at rings *C* and *D* (see the text for detail), are oriented along [011] and [01−1] to form molecular sheet at two dimensional *bc*-plane.

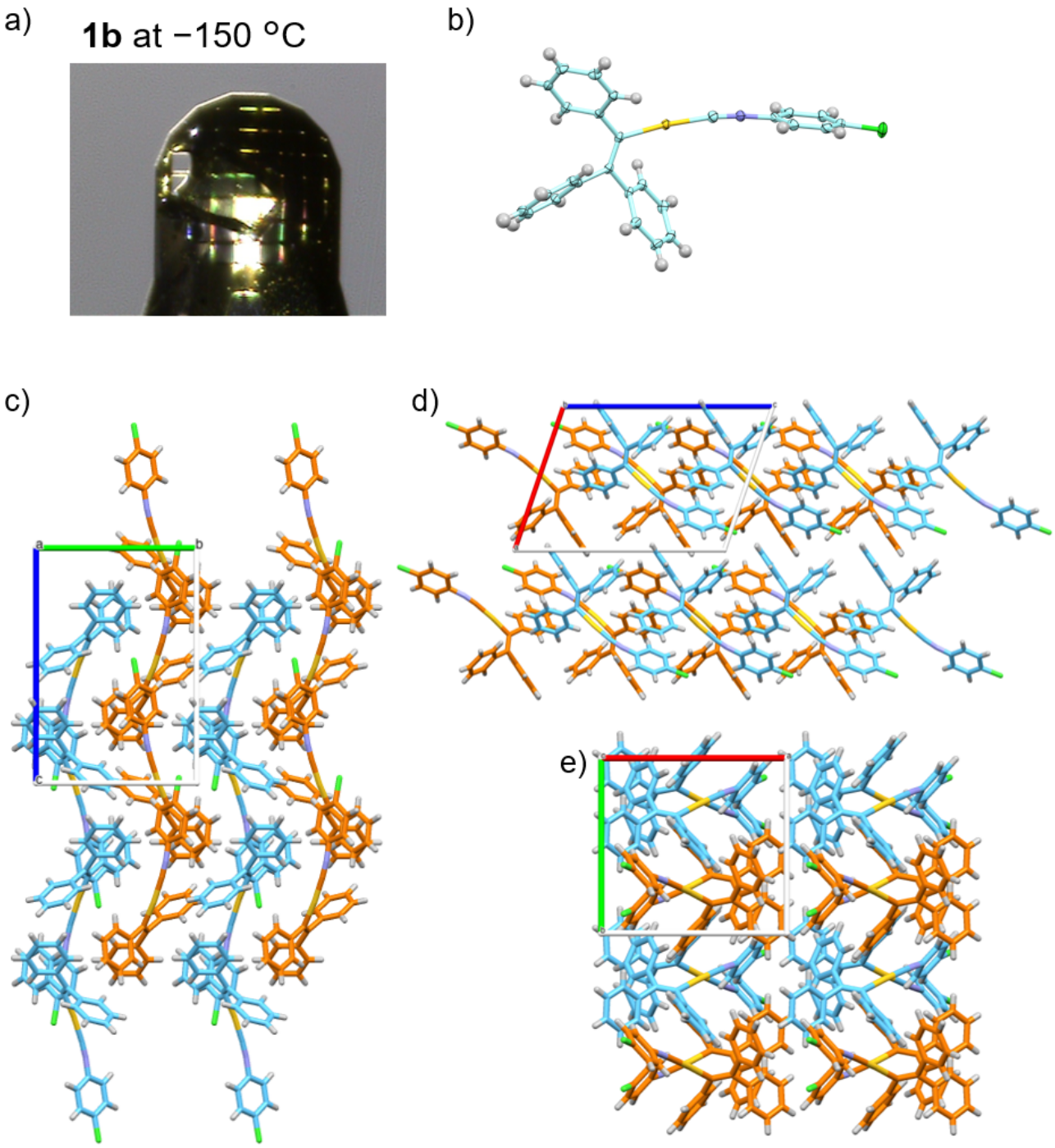

Fig. S11 a) Photograph of the single crystal of **1b** at −150 °C in which lots of Paraton oil was used to fix the crystals to decrease the probability of the crystals breaking upon cooling. Single crystal structure of **1b** at −150 °C which display b) a monomer and packing arrangements viewed along c) *a* axis, d) *b* axis, and e) *c* axis.

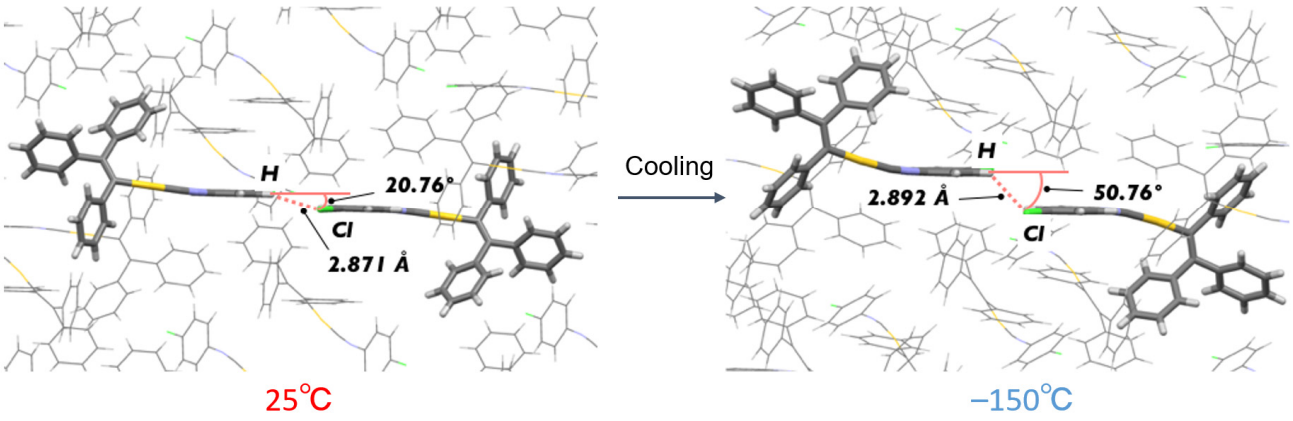

Fig. S12 Comparison of two molecules of **1** derived from the single-crystal structures of **1a** at 25 °C and **1b** at −150 °C.

Table S1. Summary of X-ray crystallographic data for **1** at 25 °C to –150 °C.

compound	**1** at 25 °C (**1a**)	**1** at 0 °C	**1** at –25 °C	**1** at –50 °C
CCDC Number	CCDC 1884311	CCDC 1884310	CCDC 1884312	CCDC 1884313
Empirical Formula	$C_{27}H_{19}AuClN$	$C_{27}H_{19}AuClN$	$C_{27}H_{19}AuClN$	$C_{27}H_{19}AuClN$
Formula Weight	589.85	589.85	589.85	589.85
Crystal Size / mm	0.3×0.2×0.05	0.3×0.2×0.05	0.3×0.2×0.05	0.3×0.2×0.05
Crystal System	monoclinic	monoclinic	monoclinic	monoclinic
a / Å	12.3955(4)	12.3778(4)	12.3580(3)	11.6176(3)
b / Å	11.0900(3)	11.0704(3)	11.0601(2)	11.5301(3)
c / Å	17.1445(5)	17.1193(5)	17.0928(4)	17.0283(5)
α / °	90	90	90	90
β / °	108.694(3)	108.640(3)	108.556(3)	108.005(3)
γ / °	90	90	90	90
V / Å^3	2232.46(12)	2222.76(11)	2214.81(10)	2169.28(11)
Space Group	$P2_1/c$ (#14)	$P2_1/c$ (#14)	$P2_1/c$ (#14)	$P2_1/c$ (#14)
Z value	4	4	4	4
D_{calc} / g cm^{-3}	1.755	1.763	1.769	1.806
Temperature / K	298	273	248	223
$2\theta_{max}$ / °	57.896	58.066	57.864	57.986
μ (Mo Kα) / cm^{-1}	67.23	67.52	67.76	69.18
No. of Reflections	Total: 22463 Unique: 5116 R_{int} = 0.0311	Total: 18937 Unique: 4966 R_{int} = 0.0287	Total: 23780 Unique: 5072 R_{int} = 0.0362	Total: 19544 Unique: 4990 R_{int} = 0.0440
R_1[a]	0.0269	0.0245	0.0253	0.0263
wR_2[b]	0.0597	0.0537	0.0706	0.0720
GOF[c]	1.026	1.028	0.984	0.878
Max./Mini. peak I[d] / Å^3	1.13 e$^-$/−0.58 e$^-$	1.03 e$^-$/−0.74 e$^-$	1.16 e$^-$/−0.86 e$^-$	0.98 e$^-$/−0.63 e$^-$

compound	**1** at –75 °C	**1** at –100 °C	**1** at –125 °C	**1** at –150 °C (**1b**)
CCDC Number	CCDC 1884306	CCDC 1884307	CCDC 1884308	CCDC 1884309
Empirical Formula	$C_{27}H_{19}AuClN$	$C_{27}H_{19}AuClN$	$C_{27}H_{19}AuClN$	$C_{27}H_{19}AuClN$
Formula Weight	589.85	589.85	589.85	589.85
Crystal System	monoclinic	monoclinic	monoclinic	monoclinic
Crystal Size / mm	0.3×0.2×0.05	0.3×0.2×0.05	0.3×0.2×0.05	0.3×0.2×0.05
a / Å	11.5535(3)	11.5041(3)	11.4695(3)	11.4311(3)
b / Å	11.5464(3)	11.5471(3)	11.5435(2)	11.5318(3)
c / Å	17.0207(4)	16.9982(4)	16.9813(4)	16.9629(4)
α / °	90	90	90	90
β / °	107.922(3)	107.843(3)	107.754(3)	107.683(3)
γ / °	90	90	90	90
V / Å^3	2160.41(10)	2149.42(10)	2141.21(9)	2130.44(9)
Space Group	$P2_1/c$ (#14)	$P2_1/c$ (#14)	$P2_1/c$ (#14)	$P2_1/c$ (#14)
Z value	4	4	4	4
D_{calc} / g cm^{-3}	1.813	1.823	1.830	1.839
Temperature / K	198	173	148	123
$2\theta_{max}$ / °	57.732	57.922	57.722	58.146
μ (Mo Kα) / cm^{-1}	69.47	69.82	70.09	70.45
No. of Reflections	Total: 21065 Unique: 5040 R_{int} = 0.0463	Total: 20085 Unique: 4999 R_{int} = 0.0325	Total: 20887 Unique: 4942 R_{int} = 0.0361	Total: 20687 Unique: 4950 R_{int} = 0.0311
R_1[a]	0.0249	0.0227	0.0213	0.0189
wR_2[b]	0.0693	0.0591	0.0505	0.0451
GOF[c]	0.903	0.937	0.999	0.919
Max./Mini. peak I[d] / Å^3	0.92 e$^-$/−0.75 e$^-$	1.06 e$^-$/−0.68 e$^-$	1.07 e$^-$/−0.76 e$^-$	1.03 e$^-$/−0.77 e$^-$

[a]: For data with $I > 2.00\sigma(I)$. [b]: For all reflection data. [c]: Goodness of Fit.

8. Temperature-dependent single crystal structure analyses of 1

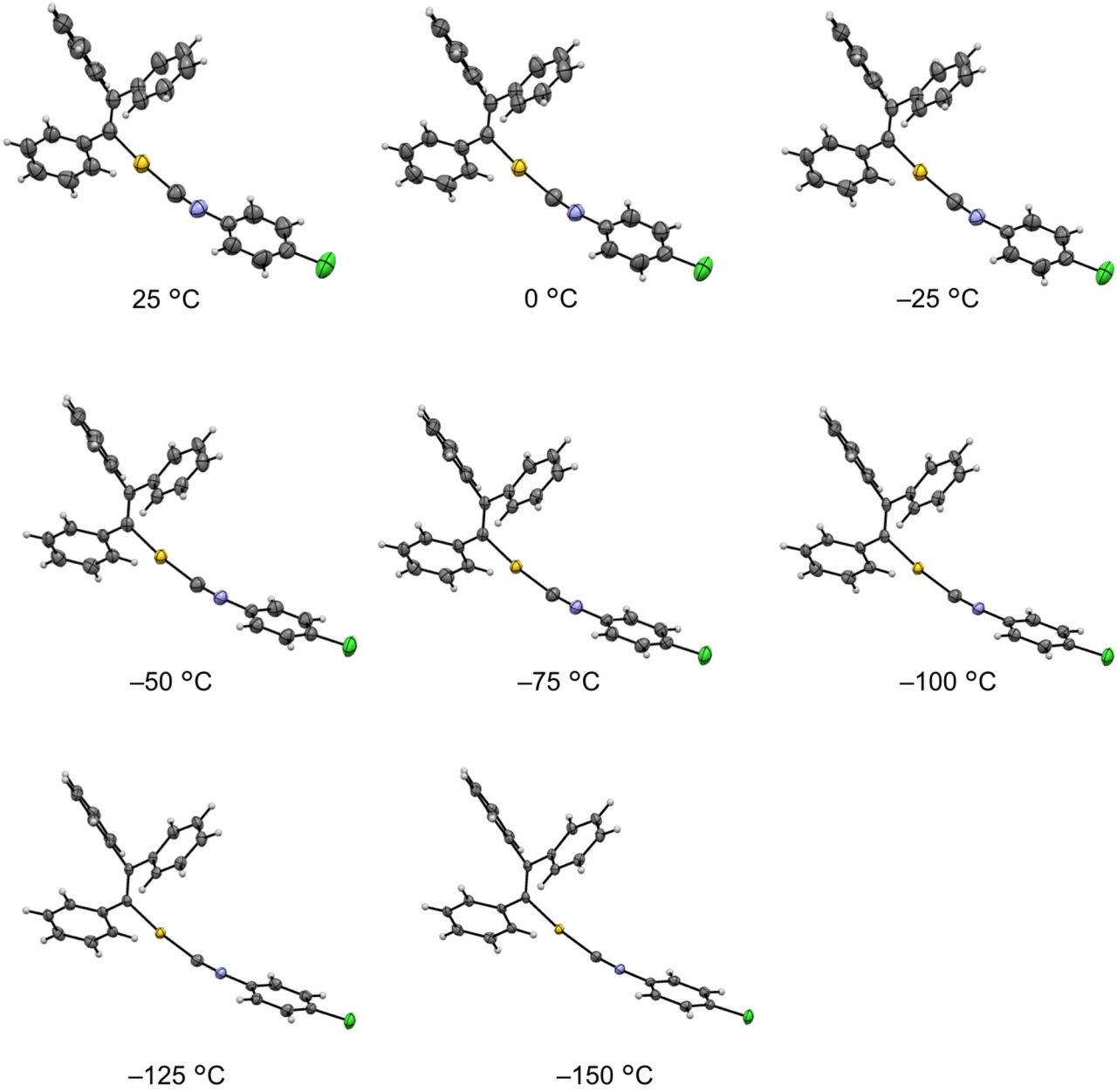

Fig. S13 Comparison of the monomers derived from the temperature-dependent sing-crystal XRD measurements from 25 °C to −150 °C.

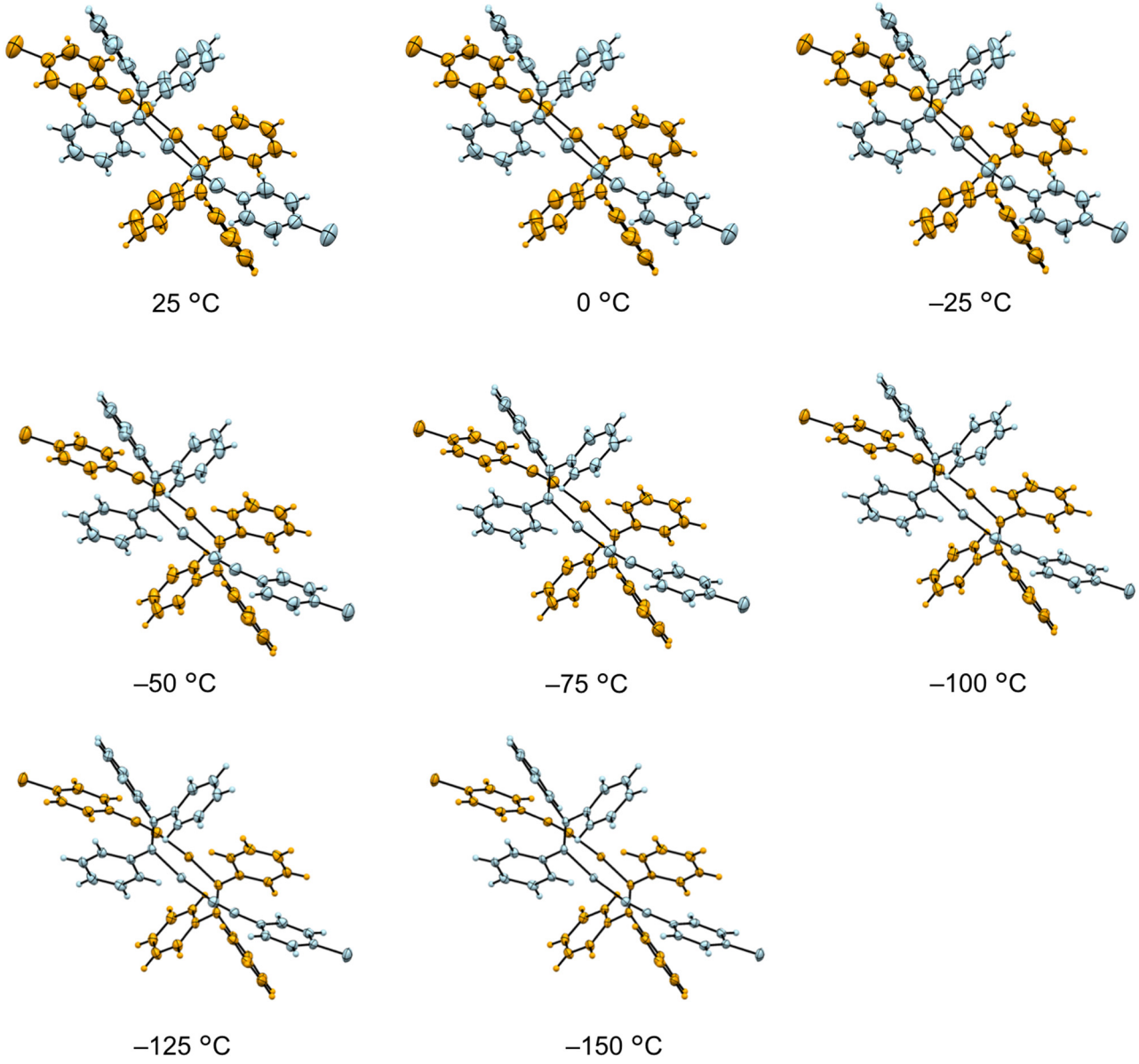

Fig. S14 Comparison of the dimers derived from the temperature-dependent single-crystal XRD measurements of **1** from 25 °C to –150 °C.

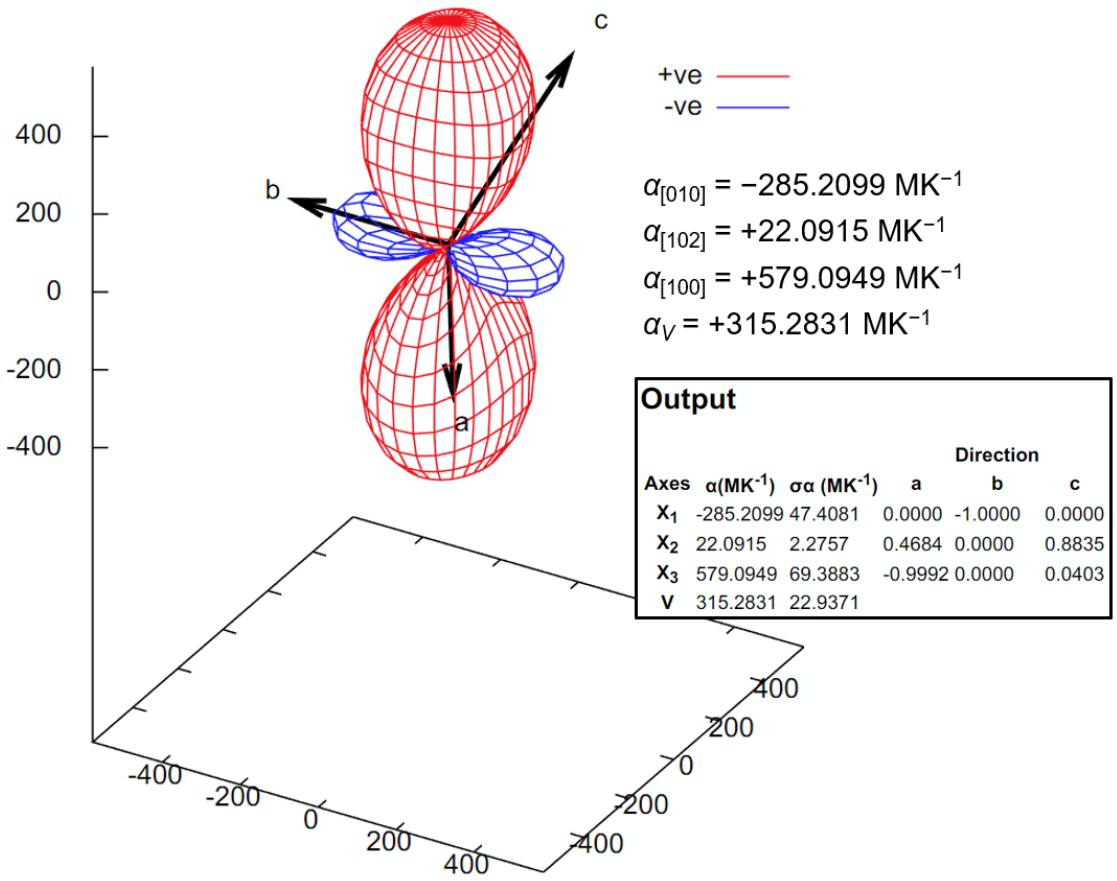

Fig. S15 Thermal expansion coefficients and plot of the expansivity indicatrices of **1** calculated using the PASCal software[3] and the following input data:

Temp.	deviation	*a*	*b*	*c*	*α*	*β*	*γ*
298	1	12.3955	11.0900	17.1445	90.000	108.694	90.000
273	1	12.3778	11.0704	17.1193	90.000	108.640	90.000
248	1	12.3580	11.0601	17.0928	90.000	108.556	90.000
223	1	11.6176	11.5301	17.0283	90.000	108.005	90.000
198	1	11.5535	11.5464	17.0207	90.000	107.922	90.000
173	1	11.5041	11.5471	16.9982	90.000	107.843	90.000
148	1	11.4695	11.5435	16.9813	90.000	107.754	90.000
123	1	11.4311	11.5318	16.9629	90.000	107.683	90.000

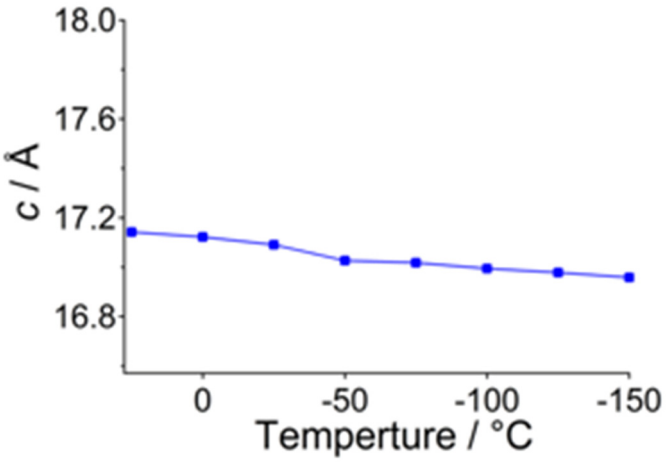

Fig. S16 Change in the length of *c* axis derived from the single-crystal XRD analyses upon temperature changes.

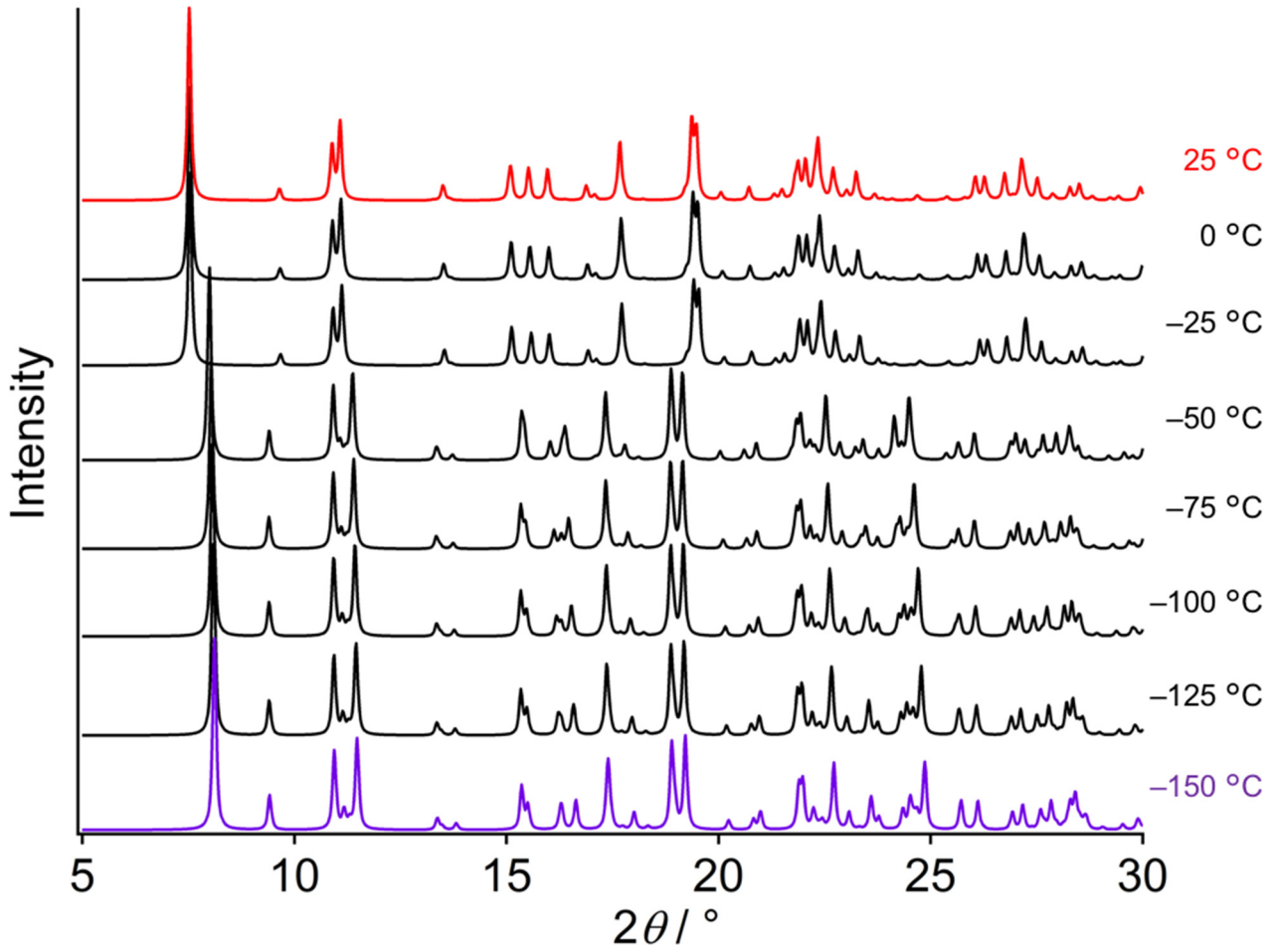

Fig. S17 Simulated powder XRD patterns derived from the temperature-dependent single-crystal XRD measurements of **1** from 25 °C to –150 °C.

9. DSC and temperature-dependent PXRD patterns of the powder forms of 1

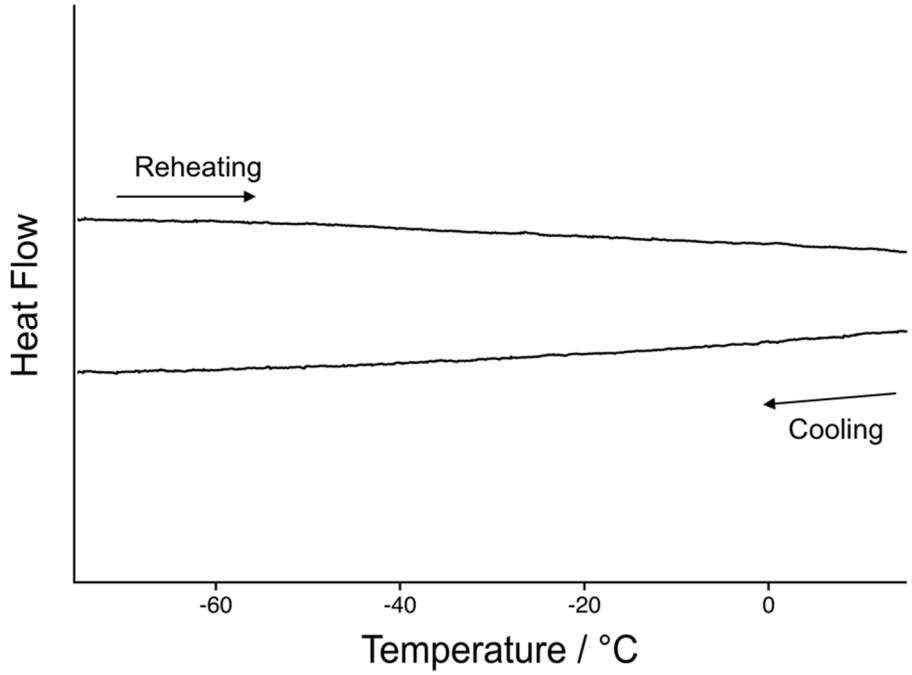

Fig. S18 DSC traces of the powder form of **1** at cooling/heating rates of 5 °C/min.

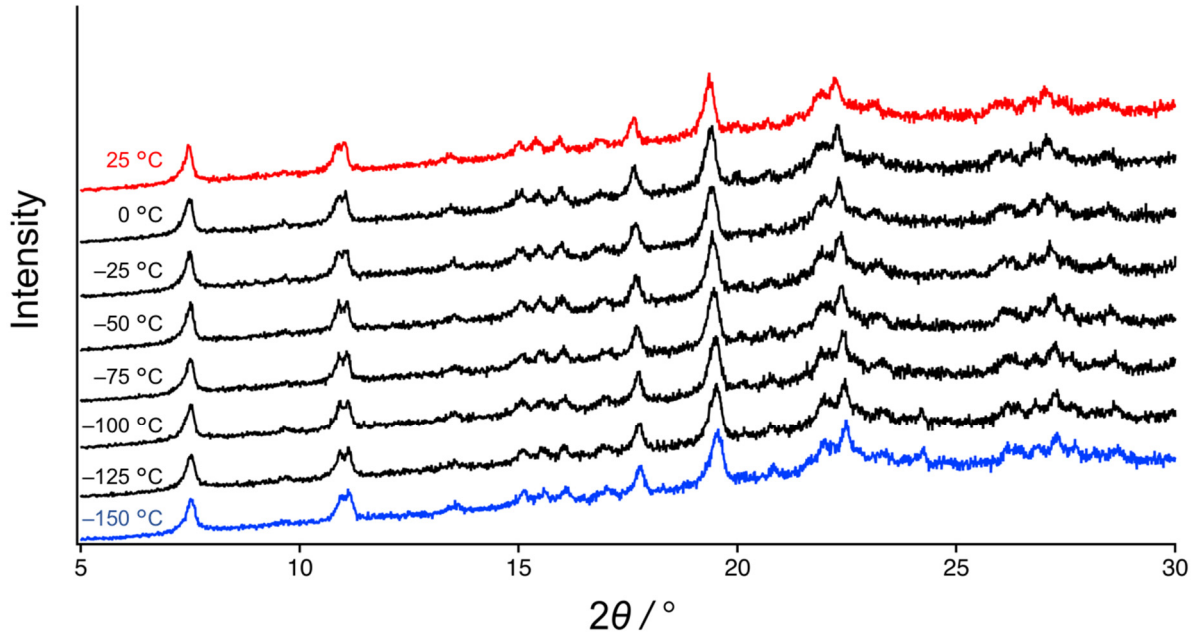

Fig. S19 Powder XRD patterns of the powder samples of **1** from 25 °C to –150 °C. The sample cooling rate between the measurements is 5 °C/min.

10. Face index experiments of 1a and 1b

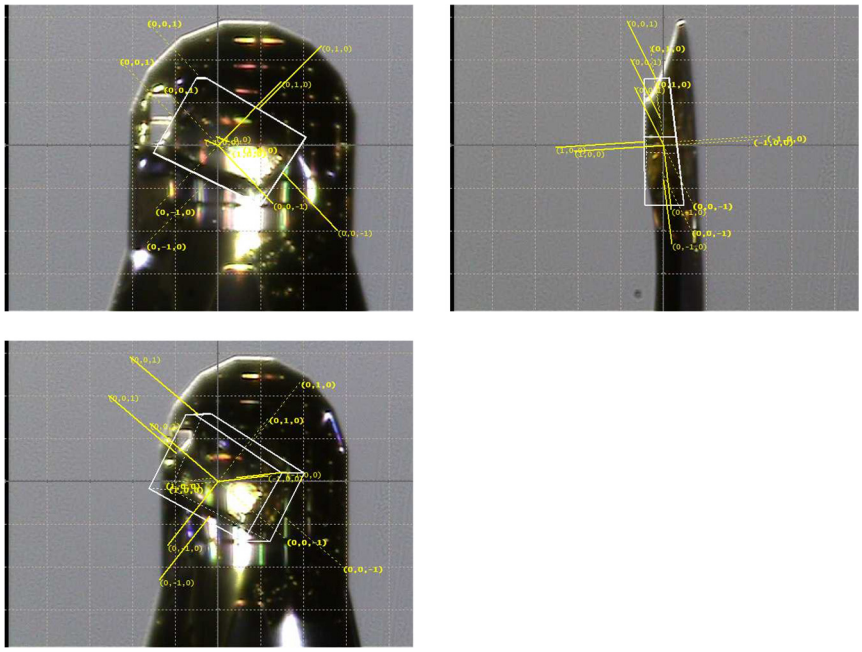

Fig. S20 Photographs showing the result of the face index measurement of the single crystal **1a** at 25 °C.

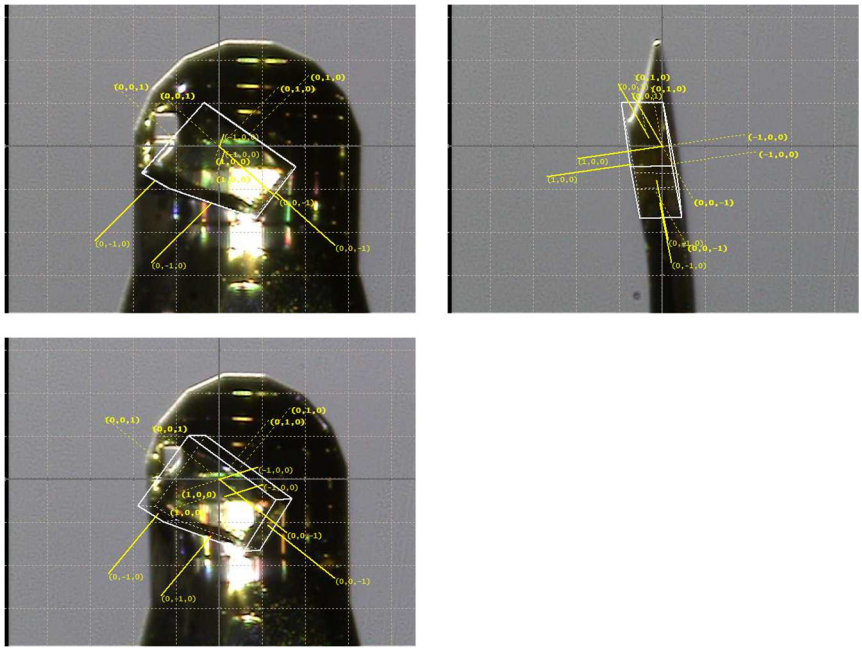

Fig. S21 Photographs showing the result of the face index measurement of the single crystal **1b** at –150 °C.

11. NMR spectra of 1

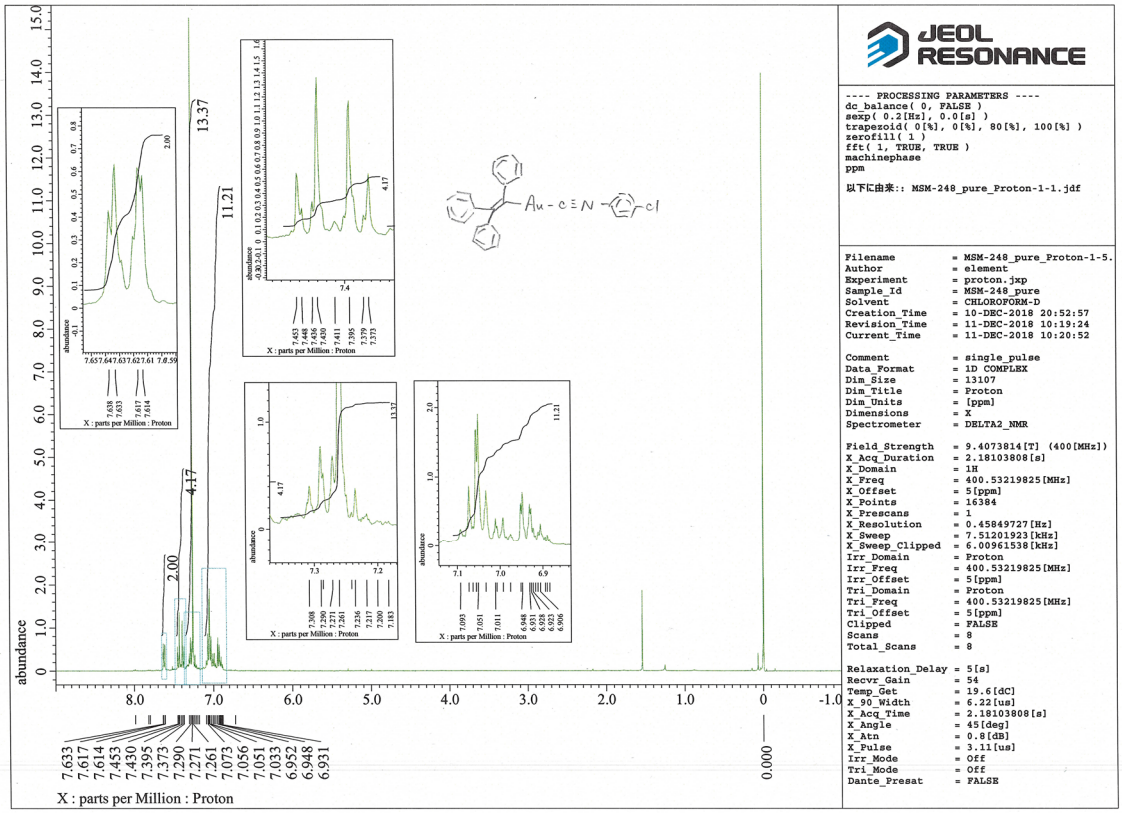

Fig. S22 ^{1}H NMR spectrum of **1** dissolved in $CDCl_3$.

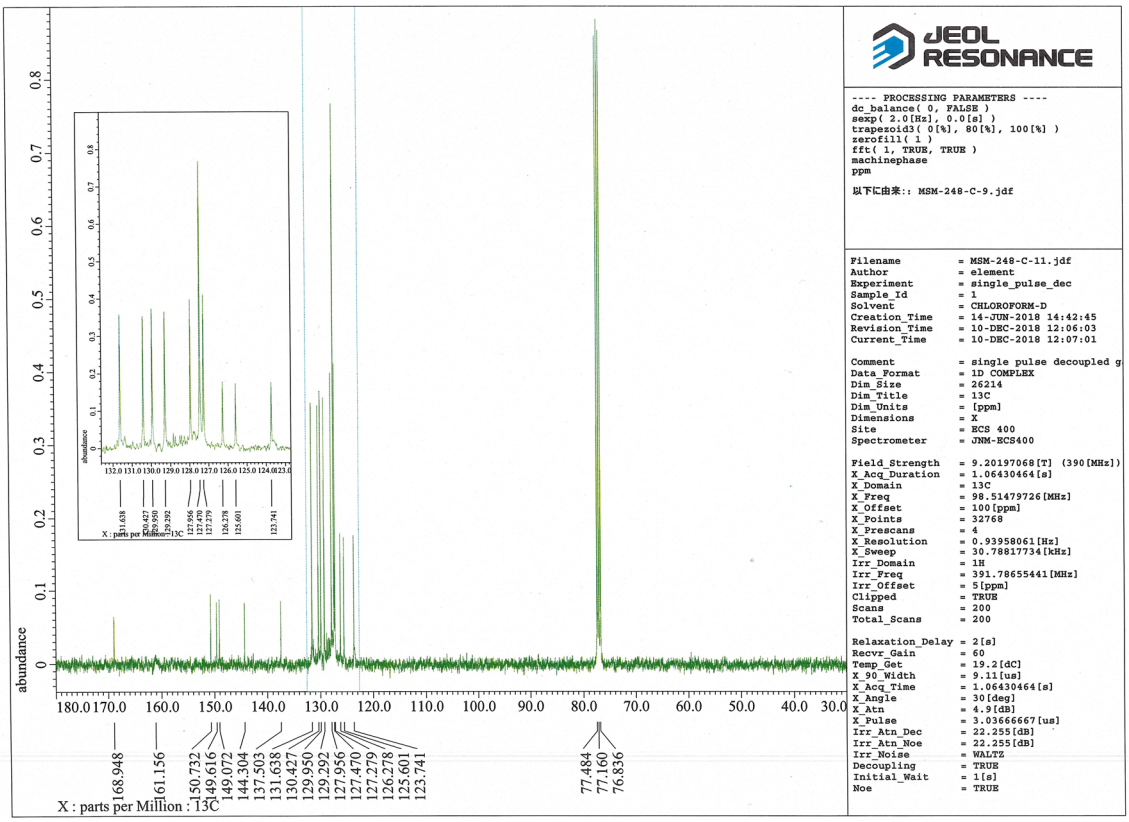

Fig. S23 ^{13}C NMR spectrum of **1** dissolved in $CDCl_3$.

12. References

1. G. M. Sheldrick *Acta Crystallogr., Sect. A* **2008**, *64*, 112.

2. https://www.ccdc.cam.ac.uk/support-and-resources/Downloads/

3. M. J. Cliffe and A. L. Goodwin, *J. Appl. Cryst.*, 2012, **45**, 1321–1329.